IEEE/CSC & ESAS SUPERCONDUCTIVITY NEWS FORUM (global edition), January 2017 (Preview 1).
Preprint of ASC 2016 manuscript 1EOr3C-03 submitted *to IEEE Trans. Appl. Supercond.* for possible publication.
DOI: 10.1109/TASC.2016.2639378.

Optimization of Transition Edge Sensor Arrays for Cosmic Microwave Background Observations with the South Pole Telescope

J. Ding, P. A. R. Ade, A. J. Anderson, J. Avva, Z. Ahmed, K. Arnold, J. E. Austermann, A. N. Bender, B. A. Benson, L. E. Bleem, K. Byrum, J. E. Carlstrom, F. W. Carter, C. L. Chang, H. M. Cho, J. F. Cliche, A. Cukierman, D. Czaplewski, R. Divan, T. de Haan, M. A. Dobbs, D. Dutcher, W. Everett, A. Gilbert, R. Gannon, R. Guyser, N. W. Halverson, N. L. Harrington, K. Hattori, J. W. Henning, G. C. Hilton, W. L. Holzapfel, J. Hubmayr, N. Huang, K. D. Irwin, O. Jeong, T. Khaire, D. Kubik, C. L. Kuo, A. T. Lee, E. M. Leitch, S. S. Meyer, C. S. Miller, J. Montgomery, A. Nadolski, T. Natoli, H. Nguyen, V. Novosad, S. Padin, Z. Pan, J. Pearson, C. M. Posada, A. Rahlin, C. L. Reichardt, J. E. Ruhl, B. R. Saliwanchik, J. T. Sayre, J. A. Shariff, I. Shirley, E. Shirokoff, G. Smecher, J. Sobrin, L. Stan, A. A. Stark, K. Story, A. Suzuki, Q. Y. Tang, R. B. Thakur, K. L. Thompson, C. Tucker, K. Vanderlinde, J. D. Vieira, G. Wang, N. Whitehorn, W. L. K. Wu, V. Yefremenko, K. W. Yoon

***Abstract*—In this paper, we describe the optimization of transition-edge-sensor (TES) detector arrays for the third-generation camera for the South Pole Telescope (SPT-3G). The camera, which contains ~16,000 detectors, will make high-angular-resolution maps of the temperature and polarization of the cosmic microwave background. Our key results are: (i) scatter in the transition temperature of Ti/Au TESs is reduced by fabricating the TESs on a thin Ti(5 nm)/Au(5 nm) buffer layer; and (ii) the thermal conductivity of the legs that support our detector islands is dominated by the SiOx dielectric in the microstrip transmission lines that run along the legs.**

***Index Terms*—Transition Edge Sensors, Superconducting**

The South Pole Telescope is supported by the National Science Foundation through grant PLR-1248097. This work is also supported by the U.S. Department of Energy. Work at Argonne National Laboratory and use of the Center for Nanoscale Materials, an Office of Science user facility, were supported by the U. S. Department of Energy, Office of Science, Office of Basic Energy Sciences, under Contract No. DE-AC02-06CH11357. Partial support is also provided by the NSF Physics Frontier Center grant PHY-1125897 to the Kavli Institute of Cosmological Physics at the University of Chicago, the Kavli Foundation and the Gordon and Betty Moore Foundation grant GBMF 947. NWH acknowledges additional support from NSF CAREER grant AST-0956135. The McGill authors acknowledge funding from the Natural Sciences and Engineering Research Council of Canada, Canadian Institute for Advanced Research, and Canada Research Chairs program. *(Corresponding author: J. Ding.)*

J. Ding, T. Khaire, R. Gannon, V. Novosad, J. Pearson and C. M. Posada are with Argonne National Laboratory, Material Science Division, Argonne, IL, USA 60439 (e-mail: dingj@anl.gov).

P. A. R. Ade and C. Tucker are with Cardiff University, Cardiff, CF24 3YB, United Kingdom.

A. J. Anderson is with Fermi National Accelerator Laboratory, Batavia, IL 60510, and Kavli Institute for Cosmological Physics, University of Chicago, Chicago, IL 60637.

J. Avva, A. Cukierman, T. de Haan, N. L. Harrington, W. L. Holzapfel, N. Huang, O. Jeong, I. Shirley, A. Suzuki, N. Whitehorn and W. L. K. Wu are with Department of Physics, University of California, Berkeley, CA 94720.

Z. Ahmed, K. D. Irwin, C. L. Kuo, K. L. Thompson and K. W. Yoon are with Kavli Institute for Particle Astrophysics and Cosmology, Stanford University, Stanford, CA 94305, Department of Physics, Stanford University, Stanford, CA 94305, SLAC National Accelerator Laboratory, Menlo Park, CA 94025.

K. Arnold is with Department of Physics, University of Wisconsin, Madison, WI. 53706.

J. E. Austermann, G. C. Hilton and J. Hubmayr are with NIST Quantum Devices Group, CO, USA 80305.

A. N. Bender, L. E. Bleem and F. W. Carter are with Argonne National Laboratory, High-Energy Physics Division, Argonne, IL, USA 60439, Kavli Institute for Cosmological Physics, University of Chicago, Chicago, IL 60637.

B. A. Benson is with Fermi National Accelerator Laboratory, Batavia, IL 60510,Kavli, Institute for Cosmological Physics, University of Chicago, Chicago, IL 60637, Department of Astronomy and Astrophysics, University of Chicago, Chicago, IL 60637.

K. Byrum, G. Wang and V. Yefremenko are with Argonne National Laboratory, High-Energy Physics Division, Argonne, IL, USA 60439

J. E. Carlstrom is with Kavli Institute for Cosmological Physics, University of Chicago, Chicago, IL 60637, Enrico Fermi Institute, University of Chicago, Chicago, IL 60637, Department of Physics, University of Chicago, Chicago, IL 60637, Argonne National Laboratory, High-Energy Physics Division, Argonne, IL, USA 60439, Department of Astronomy and Astrophysics, University of Chicago, Chicago, IL 60637.

C. L. Chang and S. Padin are with Argonne National Laboratory, High-Energy Physics Division, Argonne, IL, USA 60439, Kavli Institute for Cosmological Physics, University of Chicago, Chicago, IL 60637, Department of Astronomy and Astrophysics, University of Chicago, Chicago, IL 60637.

H. M. Cho is with SLAC National Accelerator Laboratory, Menlo Park, CA 94025.

J. F. Cliché, A. Gilbert and J. Montgomery are with Department of Physics, McGill University, Montreal, Quebec H3A 2T8, Canada.

E. M. Leitch, E. Shirokoff and Q. Y. Tang are with Kavli Institute for Cosmological Physics, University of Chicago, Chicago, IL 60637, Department of Astronomy and Astrophysics, University of Chicago, Chicago, IL 60637.

D. Czaplewski, R. Divan, S. Miller and L. Stan are with Argonne National Laboratory, Center for Nanoscale Materials, Argonne, IL, USA 60439

M. A. Dobbs is with Department of Physics, McGill University, Montreal, Quebec H3A 2T8, Canada, Canadian Institute for Advanced Research, CIFAR Program in Cosmology and Gravity, Toronto, ON, M5G 1Z8, Canada

D. Dutcher, Z. Pan and J. Sobrin are with Kavli Institute for Cosmological Physics, University of Chicago, Chicago, IL 60637, Department of Physics, University of Chicago, Chicago, IL 60637

W. Everett and J. T. Sayre are with CASA, Department of Astrophysical and Planetary Sciences, University of Colorado, Boulder, Colorado 80309, USA

R. Guyser and A. Nadolski are with Astronomy Department, University of Illinois, Urbana, IL 61801 USA

N. W. Halverson is with CASA, Department of Astrophysical and Planetary Sciences, University of Colorado, Boulder, Colorado 80309, USA, Department of Physics, University of Colorado, Boulder, CO 80309, USA.

K. Hattori is with High Energy Accelerator Research Organization (KEK), Tsukuba, Ibaraki 305-0801, Japan

J. W. Henning and R. B. Thakur are with Kavli Institute for Cosmological Physics, University of Chicago, Chicago, IL 60637.

D. Kubik, H. Nguyen and A. Rahlin are with Fermi National Accelerator Laboratory, Batavia, IL 60510

A. T. Lee is with University of California, Berkeley, CA 94720, Physics Division, Lawrence Berkeley National Laboratory, Berkeley, CA 94720.

S. S. Meyer is with Kavli Institute for Cosmological Physics, University of Chicago, Chicago, IL 60637, Enrico Fermi Institute, University of Chicago, Chicago, IL 60637, Department of Physics, University of Chicago, Chicago,

IEEE/CSC & ESAS SUPERCONDUCTIVITY NEWS FORUM (global edition), January 2017 (Preview 1).
Preprint of ASC 2016 manuscript 1EOr3C-03 submitted *to IEEE Trans. Appl. Supercond.* for possible publication.
DOI: 10.1109/TASC.2016.2639378.

Detectors, Bolometers, Cosmic Microwave Background, South Pole Telescope.

I. Introduction

Current cosmic microwave background (CMB) [1], [2] experiments aim to precisely measure the CMB polarization, especially the parity-violating B-mode polarization, [3] with the goal of measuring the energy scale of inflation, the number of neutrino species, and the sum of masses of neutrinos. [4], [5] The measurements require exquisite sensitivity, which means large-format cameras with many bands for removing foreground signals. [6] One such camera, which is being built for the next-generation experiment on the South Pole Telescope (SPT-3G), [7] has 2690 pixels, each with 6 transition-edge sensor (TES) detectors [8], [9] measuring 2 linear polarizations in 3 bands, and will be deployed at the end of 2016.

In this paper, we describe the optimization of the TES detector arrays for SPT-3G. The TES critical temperature (T_c) distributions of wafers prepared by two different detector fabrication processes and two different TES film structures have been systematically investigated. The result shows that the TES performance becomes more controllable if the TES is prepared on an unetched surface with a thin Ti(5 nm)/Au(5 nm) buffer layer. The thermal link, a LSN(low-stress silicon nitride)/Nb/SiOx/Nb quadruple layer structure, is another critical component for the detector array. Two test wafers were fabricated to investigate the detailed thermal link properties as functions of the film structure and the leg dimensions. We found that the thermal conductance is approximately linearly dependent on the leg width-to-length ratio in our detector arrays, and the LSN contributes approximately 30% of the total thermal conductance of the whole leg. These results provide important information for improving the overall sensitivity of the detector array.

The paper is organized as follows: Section II gives an overview of the detector fabrication and characterization, Section III describes the TES performance with different substrate surfaces and film structures, and Section IV describes an investigation of the thermal link properties.

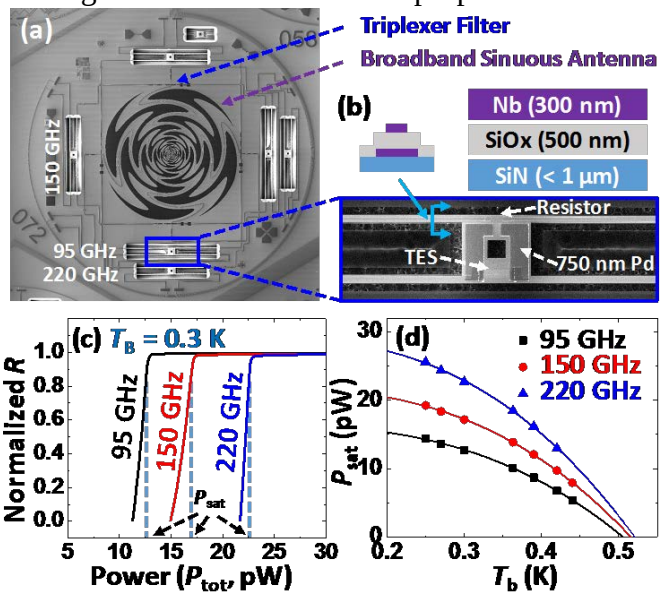

Fig. 1. (a) SEM image of a pixel. (b) Detail around the island. All TESs are with a dimension of 15 μm× 80μm in this paper. The sketch shows the cross-section of a leg. The LSN layer was 1μm before processing and it will be thinner in the final devices. (c) TES resistance as a function of the P_{tot} for different bands. (d) P_{sat} as a function of the Bath Temperature T_b: measurements (points) and predicted trend (solid curves).

II. Detector Design and Characterization

A. Design

The SPT-3G camera has 10 hexagonal detector arrays, each containing 269 pixels. Fig. 1(a) shows the details of a pixel. The millimeter-wavelength signal is received by a self-complementary, log-periodic, broadband, sinuous antenna. [10], [11] Three-pole, quasi-lumped-element filters [12]–[14] split the signal into three bands centered around 95, 150 and 220 GHz. Superconducting, 10 Ω, Nb, microstrip, transmission lines [15] distribute the balanced signal for each band to the appropriate detector island, where it is absorbed by a 20 Ω Ti/Au load resistor. The change in temperature of the island is then sensed by a Ti/Au TES. A 750 nm thick layer of Pd is deposited on the island to

IL 60637, Department of Astronomy and Astrophysics, University of Chicago, Chicago, IL 60637

T. Natoli is with Dunlap Institute for Astronomy & Astrophysics, University of Toronto, Toronto, ON, M5S 3H4, Canada.

C. L. Reichardt is with School of Physics, University of Melbourne, Parkville, 3010.

J. E. Ruhl, B. R. Saliwanchik and J. A. Shariff are with Physics Department, Case Western Reserve University, Cleveland, OH 44106.

G. Smecher is with Three-Speed Logic, Inc., Vancouver, B.C., V6A 2J8, Canada.

A. A. Stark is with Harvard-Smithsonian Center for Astrophysics, Cambridge, MA 02138.

K. Story is with Kavli Institute for Particle Astrophysics and Cosmology, Stanford University, Stanford, CA 94305, Department of Physics, Stanford University, Stanford, CA 94305.

K. Vanderlinde is with Dunlap Institute for Astronomy & Astrophysics, University of Toronto, Toronto, ON, M5S 3H4, Canada, Department of Astronomy & Astrophysics, University of Toronto, Toronto, ON, M5S 3H4, Canada

J. D. Vieira is with Astronomy Department, University of Illinois, Urbana, IL 61801 USA, Department of Physics,University of Illinois, Urbana, IL 61801 USA.

DOI: 10.1109/TASC.2016.2639378.

increase the heat capacity and stabilize the detector. [16] The thermal link of the TES detector is a set of four LSN legs that support the island. The leg length and width is designed to provide a detector saturation power (P_{sat}) roughly 2.5 times the expected loading (P_{load}) from the sky, telescope, and cold optics. Detailed information about the island and the leg are shown in Fig. 1(b). Fabrication details for the SPT-3G detector arrays are given in Posada et al.. [17], [18]

B. Characterization

A digital, frequency-domain, multiplexing scheme [19] has been developed to read out groups of 64 detectors using a single pair of wires, [20] makeing it possible to quickly evaluate the performance of large numbers of detectors.

For this work, the detector performance was investigated using measurements of the resistance, (R), versus P_{sat} for different bath (i.e., wafer or wafer holder) temperatures (T_b) as shown in Fig. 1(c). $P_{sat}(T_b)$ is indicated by the dashed lines in Fig. 1(c). Values of $P_{sat}(T_b)$ from Fig. 1(c) can be plotted, as in Fig. 1(d), and fitted to: [21]–[23]

$$P_{sat} = K\cdot(T_c^{\,n} - T_b^{\,n}) \qquad (1)$$

where the constant $K = NkA/l$, N is the number of legs, A is the leg cross section, l is the leg length, k is the thermal conductivity of the leg material, and, n is the index for thermal conductivity. The fit yields values of the parameters and the thermal conduction ratio $G(T_c) = dP_{sat}/dT = nKT_c^{\,n-1}$. Since the phonon noise equivalent power (NEP) [24] is directly related to G and T_c, it is important to keep P_{sat} within a reasonable range.

Currently in SPT-3G project, the target T_c is 510 mK and the target P_{sat} is 10.6 pW, 16.0 pW and 21.0 pW for 95 GHz, 150 GHz and 220 GHz bands, respectively. These values are equal to twice the expected optical loading during normal operation, assuming an overall optical efficiency of 85%. They may be varied depending on the measured optical efficiency.

III. TES PERFORMANCE

In some SPT-3G arrays, the TESs are fabricated on an etched SiOx surface, [17] while in others, the TESs are fabricated on an unetched surface. [18] The unetched surface gives much lower scatter in T_c, as shown in Figs. 2(a) and (b). It is possible that residual by-products and increased roughness, due to etching SiOx during fabrication of the Nb microstrip, may cause the large scatter shown in Fig. 2(a). The TESs on etched SiOx have slightly higher T_c than those on unetched SiOx, due to the fact that the latter are prepared at a much earlier stage, so they encounter more fabrication processing. Heating during processing reduces the TES T_c, as shown in the inset in Fig. 2(b).

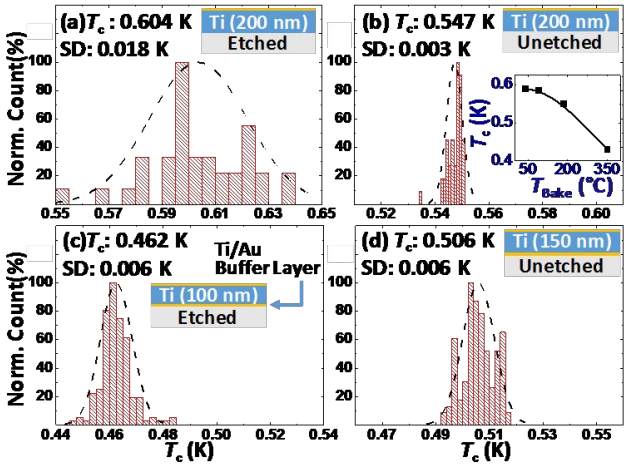

Fig. 2. T_c distribution for TESs (a) on etched SiOx, (b) on unetched SiOx, (c) with Ti(5nm)/Au(5nm) buffer layer on etched SiOx, (d) with Ti(5nm)/Au(5nm) buffer layer on unetched SiOx. TES T_c change as a function of the baking temperature (T_{Bake}) is shown in the insert of (b). The average T_c and standard deviation (SD) are labeled in each figure. All TESs are covered by 20 nm Au in this paper.

We have also investigated adding a Ti(5 nm)/Au(5 nm) buffer layer under the TES to isolate the TES from the substrate. The buffer layer results in lower T_c, and lower scatter in T_c, for both etched and unetched SiOx, as shown in Figs. 2(c) and 2(d). In Figs. 2(c) and 2(d) the combination of the buffer layer and thinner Ti (100 nm for Fig. 2(c) and 150 nm for Fig. 2(d)) gives T_c in the range 450 - 510 mK, cf. 550-600 mK for the thicker TESs without buffer layer in Figs. 2(a) and 2(b).

The small scatter in T_c in Fig. 2(b) may be due to a smaller number of detectors for this measurement (~50 for Figs. 2(a) and 2(b), cf. ~150 for Figs. 2(c) and 2(d)) or variations in the etch that releases the detector legs and islands from the Si wafer (releasing process). Releasing decreases T_c, probably due to heating of the TESs, and increases the scatter in T_c, as shown in Fig. 3. Fig. 3 also shows a larger variation in T_c with radius and band. Since these effects are only observed in released devices, they could be due to (i) excess, band-dependent, optical loading in the measurement

Preprint of ASC 2016 manuscript 1EOr3C-03 submitted *to IEEE Trans. Appl. Supercond.* for possible publication.
DOI: 10.1109/TASC.2016.2639378.

setup, or (ii) heating of the TESs during release (or during final oxygen plasma cleaning to remove photoresist), which may depend on band because detectors for different bands have different leg lengths with different thermal conductivities.

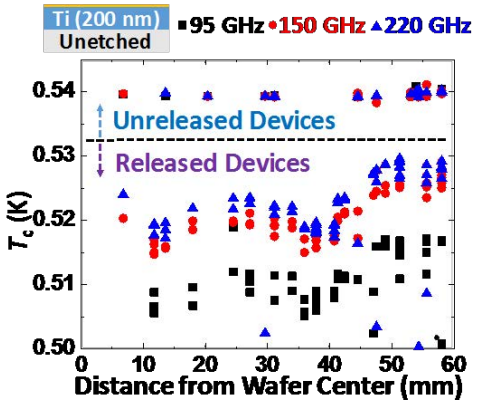

Fig. 3. TES T_c as a function of the distance from the wafer center for unreleased detectors (top panel) and released detectors (bottom panel, the detector legs and islands are released from the Si wafer). Every 4th row of pixelss on this wafer was left unreleased.

IV. Properties of the Thermal Link

We have fabricated two test wafers to investigate the effects of different film structures (Fig. 4(a-c)) and different leg widths and lengths (Fig. 4(d-f)), respectively. Fig. 4(a-c) shows results for detectors with (a) legs that have only LSN and Nb leads for reading out the TESs (black squares), (b) legs with LSN, the 500 nm SiOx dielectric for microstrip transmission line and Nb leads (blue dots), and (c) legs that have LSN and a complete microstrip transmission line (red triangles). K for detectors with only LSN and Nb leads is 3 times smaller than for the other configurations, and the microstrip Nb ground layer has little effect on K, as expected for a superconductor, so the thermal conductivity of the legs must be dominated by the SiOx layer, with the LSN contributing only ~30%.

Since the SiOx layer thickness is constrained by the filter design, and the LSN layer on the legs must be thick enough to support the island without breaking, changes to the leg thermal conductivity may require a different leg width or length. Fig. 4(d-f) shows measurements of detectors from a wafer on which ¼ of the detectors have 23% longer legs and ¼ have 26% narrower legs. A complete discussion of these results is outside the scope of this paper (more discussion about thermal link can be found in [25], [26]) and the origin of the scattering of K in our results is still under investigation. However, it is clear that K is approximately proportional to the ratio of leg width to leg length (W/L), as expected for long legs. The scaling of K with W/L also suggests that the islands and legs are fully released, i.e., the legs are the only thermal link between island and the substrate. A touch between island and the substrate would give a higher K for long and narrow legs than the observed results.

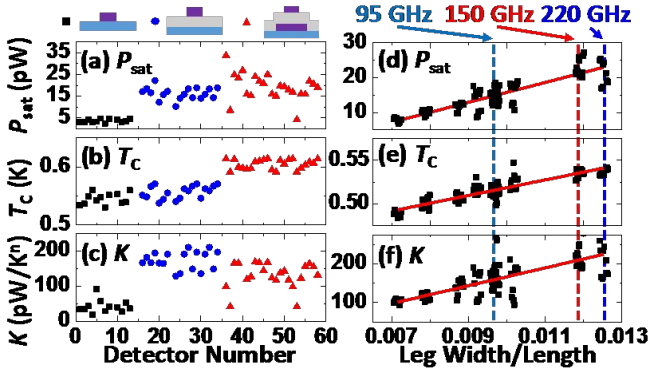

Fig. 4. Detector parameters for different leg film configurations (a-c), and different leg widths and lengths (d-f). For these measurements, T_b =300 mK. The detectors in (a-c) are dark (no load resistors on the islands).

V. Conclusion

In summary, we have shown that adding a thin Ti(5 nm)/Au(5 nm) buffer layer under a Ti/Au TES significantly decreases the scatter in transition temperature. We have demonstrated that the thermal conductivity of the legs that support the SPT-3G detector islands is dominated by the SiOx microstrip dielectric layer, and that the thermal conductivity scales as expected with leg width/length. These results will be used to optimize the performance of the TES detector arrays for the new SPT-3G camera.

References

[1] A. A. Penzias and R. W. Wilson, "A Measurement of Excess Antenna Temperature at 4080 Mc/s.," *Astrophys. J.*, vol. 142, p. 419, Jul. 1965.

[2] R. H. Dicke, P. J. E. Peebles, P. G. Roll, and D. T. Wilkinson, "Cosmic Black-Body Radiation.," *Astrophys. J.*, vol. 142, no. 9, p. 414, Jul. 1965.

[3] D. Hanson et al., "Detection of B-Mode Polarization in the Cosmic Microwave Background with Data from the South Pole Telescope," *Phys. Rev. Lett.*, vol. 111, no. 14, p. 141301, Sep. 2013.

[4] K. N. Abazajian et al., "Neutrino physics from the cosmic microwave background and large scale structure," *Astropart. Phys.*, vol. 63, pp. 66–80, Mar. 2015.

[5] W. Hu and T. Okamoto, "Mass Reconstruction with Cosmic Microwave Background Polarization," *Astrophys. J.*, vol. 574, no. 2, pp. 566–574, Aug. 2002.

[6] J. Bock et al., "Task Force on Cosmic Microwave Background Research," *arXiv:astro-ph/0604101*, Apr. 2006.

[7] B. A. Benson et al., "SPT-3G: a next-generation cosmic microwave background polarization experiment on the South Pole telescope," in *Proc. SPIE 9153, Millimeter, Submillimeter, and Far-Infrared*

DOI: 10.1109/TASC.2016.2639378.

Detectors and Instrumentation for Astronomy VII, vol. 9153, p. 91531P, 2014.

[8] K. D. Irwin, "An application of electrothermal feedback for high resolution cryogenic particle detection," *Appl. Phys. Lett.*, vol. 66, no. 15, p. 1998, 1995.

[9] A. T. Lee, P. L. Richards, S. W. Nam, B. Cabrera, and K. D. Irwin, "A superconducting bolometer with strong electrothermal feedback," *Appl. Phys. Lett.*, vol. 69, no. 12, p. 1801, 1996.

[10] R. H. Duhamel, "Dual Polarized Sinuous Antennas," US 4658262 A, 1987.

[11] J. M. Edwards, R. O'Brient, A. T. Lee, and G. M. Rebeiz, "Dual-Polarized Sinuous Antennas on Extended Hemispherical Silicon Lenses," *IEEE Trans. Antennas Propag.*, vol. 60, no. 9, pp. 4082–4091, Sep. 2012.

[12] S. Kumar et al., "Millimeter-Wave Lumped Element Superconducting Bandpass Filters for Multi-Color Imaging," *IEEE Trans. Appl. Supercond.*, vol. 19, no. 3, pp. 924–929, Jun. 2009.

[13] R. O'Brient et al., "A dual-polarized broadband planar antenna and channelizing filter bank for millimeter wavelengths," *Appl. Phys. Lett.*, vol. 102, no. 6, p. 63506, 2013.

[14] A. Suzuki et al., "Multi-chroic Dual-Polarization Bolometric Focal Plane for Studies of the Cosmic Microwave Background," *J. Low Temp. Phys.*, vol. 167, no. 5–6, pp. 852–858, Jun. 2012.

[15] C. L. Chang et al., "Low Loss Superconducting Microstrip Development at Argonne National Lab," *IEEE Trans. Appl. Supercond.*, vol. 25, no. 3, pp. 1–5, Jun. 2015.

[16] K. D. Irwin, G. C. Hilton, D. A. Wollman, and J. M. Martinis, "Thermal-response time of superconducting transition-edge microcalorimeters," *J. Appl. Phys.*, vol. 83, no. 8, p. 3978, 1998.

[17] C. M. Posada et al., "Fabrication of large dual-polarized multichroic TES bolometer arrays for CMB measurements with the SPT-3G camera," *Supercond. Sci. Technol.*, vol. 28, no. 9, p. 94002, Sep. 2015.

[18] C. M. Posada et al., "Large arrays of dual-polarized multichroic TES detectors for CMB measurements with the SPT-3G receiver," in *Proc. SPIE 9914, Millimeter, Submillimeter, and Far-Infrared Detectors and Instrumentation for Astronomy VIII*, vol. 9914, p. 991417, 2016.

[19] A. N. Bender et al., "Digital frequency domain multiplexing readout electronics for the next generation of millimeter telescopes," in *SPIE Astronomical Telescopes + Instrumentation*, vol. 9153, p. 91531A, 2014.

[20] A. N. Bender et al., "Integrated performance of a frequency domain multiplexing readout in the SPT-3G receiver," in *SPIE 9914, Millimeter, Submillimeter, and Far-Infrared Detectors and Instrumentation for Astronomy VIII*, vol. 9914, p. 99141D, 2016.

[21] A. D. Turner et al., "Silicon nitride micromesh bolometer array for submillimeter astrophysics," *Appl. Opt.*, vol. 40, no. 28, p. 4921, Oct. 2001.

[22] M. Kenyon, P. K. Day, C. M. Bradford, J. J. Bock, and H. G. Leduc, "Electrical Properties of Background-Limited Membrane-Isolation Transition-Edge Sensing Bolometers for Far-IR/Submillimeter Direct-Detection Spectroscopy," *J. Low Temp. Phys.*, vol. 151, no. 1–2, pp. 112–118, Apr. 2008.

[23] K. Rostem, D. M. Glowacka, D. J. Goldie, and S. Withington, "Thermal conductance measurements for the development of ultra low-noise transition-edge sensors with a new method for measuring the noise equivalent power," in *Proceedings of the SPIE - The International Society for Optical Engineering*, vol. 7020, p. 70200L, 2008.

[24] J. C. Mather, "Bolometer noise: nonequilibrium theory," *Appl. Opt.*, vol. 21, no. 6, p. 1125, Mar. 1982.

[25] G. Wang et al., "Thermal Properties of Silicon Nitride Beams Below One Kelvin," *IEEE Trans. Appl. Supercond.*, vol. 21, no. 3, pp. 232–235, Jun. 2011.

[26] K. Rostem et al., "Precision control of thermal transport in cryogenic single-crystal silicon devices," *J. Appl. Phys.*, vol. 115, no. 12, p. 124508, Mar. 2014.